Non-Fermi Liquid Behavior and Continuously Tunable Resistivity Exponents in the Anderson-Hubbard Model at Finite Temperature

Niravkumar D. Patel,[1] Anamitra Mukherjee,[2] Nitin Kaushal,[1] Adriana Moreo,[1,3] and Elbio Dagotto[1,3]
[1]*Department of Physics and Astronomy, The University of Tennessee, Knoxville, Tennessee 37996, USA*
[2]*School of Physical Sciences, National Institute of Science Education and Research, HBNI, Jatni 752050, India*
[3]*Materials Science and Technology Division, Oak Ridge National Laboratory, Oak Ridge, Tennessee 37831, USA*
(Received 17 February 2017; revised manuscript received 31 May 2017; published 24 August 2017)

We employ a recently developed computational many-body technique to study for the first time the half-filled Anderson-Hubbard model at finite temperature and arbitrary correlation U and disorder V strengths. Interestingly, the narrow zero temperature metallic range induced by disorder from the Mott insulator expands with increasing temperature in a manner resembling a quantum critical point. Our study of the resistivity temperature scaling T^{α} for this metal reveals non-Fermi liquid characteristics. Moreover, a continuous dependence of α on U and V from linear to nearly quadratic is observed. We argue that these exotic results arise from a systematic change with U and V of the "effective" disorder, a combination of quenched disorder and intrinsic localized spins.

DOI: 10.1103/PhysRevLett.119.086601

A hallmark of a conventional Fermi liquid (FL) in good metals is the T^2 scaling of the resistivity ρ with temperature T. However, deviations from this behavior have been reported in several correlated electronic materials such as heavy fermions [1–4], rare earth nickelates [5], layered dichalcogenides [6], and cuprates [7–9]. Various ideas for explaining non-Fermi liquid (NFL) states have been proposed. For instance, a $T = 0$ quantum critical point could induce the linear $\rho \sim T$ scaling in the cuprates [9–11]. In the NFL observed in the two-dimensional electron gas (2DEG) [12–14], charge or spin glassy metallic states could provide an alternative [15–18]. In spite of these important efforts, the understanding of NFLs in correlated systems still eludes theorists. Moreover, in heavy fermion experiments a puzzling continuous variation of the ρ versus T scaling exponent α between 1 and 1.6 was found [1–4]. Considering that the microscopic physics of the several NFL material families are quite different, it is a challenge to find a global understanding of NFL states in correlated systems. In particular, we need to identify concrete model Hamiltonian systems that not only support NFL states but also, within a single framework, capture various NFL systematics observed across different material families.

To address these issues, here we study the temperature characteristics of the unconventional metal known to develop at $T = 0$ from the competition between strong electron interactions and disorder in the half-filled Anderson-Hubbard model on a square lattice. In the clean limit, the ground state is a Mott insulator (MI) and correlated metals arising from doping MIs [19] violate the $\rho \sim T^2$ scaling. In the other limit where quenched disorder dominates, single particle states are localized in two dimensions and these disorder-induced Anderson insulators often display variable range hopping behavior [20].

The surprising $T = 0$ intermediate metallic state that results from the combination of correlations and disorder has been studied theoretically using statistical dynamical mean field theory [21–26], quantum Monte Carlo calculations [27–29], exact diagonalization [30], Hartree-Fock [31] and typical medium theory [32], and its cluster extensions [33], which allows direct identification of Anderson localized states.

Experimental results [6,34–37] are compatible with the zero temperature calculations. However, the finite temperature understanding of this exotic metal and its scaling is limited and several questions remain. How does a metal that arises from competing Mott and Anderson insulators behave at finite temperatures? What temperature scaling does the resistivity of the ensuing metal display? Is there a dependence of the exponent α on disorder and interaction strengths that can be tuned? Are spin or charge cluster states [18] responsible for such scaling behavior? Answers to these open questions are of relevance for experiments and theory alike.

In this Letter, we study the half-filled Anderson-Hubbard model at finite temperature using the recently developed mean field Monte Carlo (MFMC) technique. This approach properly incorporates thermal fluctuations in a mean field theory [38]. Details and benchmarks are in Sec. I of the Supplemental Material [39]. Using the MFMC technique, here we establish the disorder-interaction-temperature (V-U-T) phase diagram. In particular, we observed a disorder-induced continuous evolution from the Mott to the Anderson insulators with a strange metal in between. Our temperature analysis of this region unveils an intriguing quasi–quantum critical point behavior, with a narrow metallic region increasing in width with increasing temperature resembling a quantum phase transition.

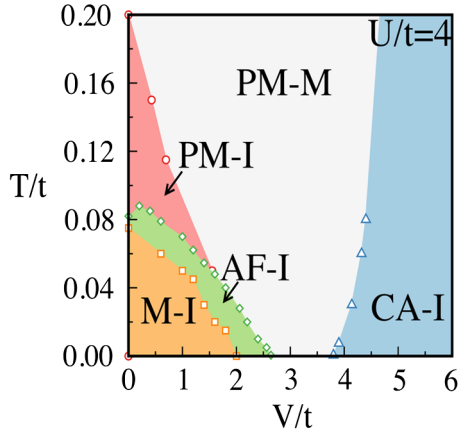

FIG. 1. Temperature T versus disorder V phase diagram at half filling for $U/t = 4.0$ obtained using a 32^2 square lattice. The zero temperature AFM Mott insulator (MI) to gapless AFM insulator (AFI) at $V \sim 2t$, and the subsequent transition to the paramagnetic metal (PMM) at $V \sim 3t$, are both continuous within our accuracy. For $V > 3.8t$ at $T = 0$, we observe a disorder-induced correlated Anderson insulator (CAI). Finally, for $T/t \in [0.08, 0.2]$ and small V/t, pink region, we find a gapless PM insulator (PMI). Details are in the text.

Through optical conductivity and resistivity calculations, we uncover a striking behavior: by changing U and V, α can be tuned (akin to heavy fermions) from linear $\alpha = 1$, as in cuprates, to near quadratic. Then, disorder and interactions can be used to modify the scaling $\rho \sim T^{\alpha}$.

The model is

$$H = -t\sum_{\langle i,j\rangle\sigma} c^{\dagger}_{i,\sigma}c_{j,\sigma} + \sum_i U n_{i\uparrow}n_{i\downarrow} + \sum_i (V_i - \mu)(n_{i\uparrow} + n_{i\downarrow}),$$

where the first term is the kinetic energy and the second is the standard Hubbard repulsion. $c_{i\sigma}$ ($c^{\dagger}_{i\sigma}$) annihilates (creates) an electron at site i with spin σ. The number operator is $n_{i\sigma} = c^{\dagger}_{i\sigma}c_{i\sigma}$. The disorder V_i at each site is chosen randomly in the interval $[-V, V]$ with uniform probability. The chemical potential μ is adjusted to achieve half filling globally. In the MFMC technique, we first Hubbard-Stratonovich decouple the interaction term, by introducing vector $\mathbf{m}_i$ and scalar ϕ_i auxiliary fields at every site. The former couples to spin and the latter to charge. Dropping the time dependence of the auxiliary fields (AFs) a model with "spin fermion" characteristics arises. The AFs are treated by classical MC calculations that admit thermal fluctuations, and the fermionic sector is solved using exact diagonalization. Details of the considerable numerical effort involved are discussed in Sec. I of the Supplemental Material [39].

Phase diagram.—Consider the phase diagram shown in Fig. 1 at the representative value $U/t = 4$. Various indicators, such as the (π, π) static magnetic structure factor [52], density of states (DOS), and optical conductivity $\sigma(\omega)$ were used (Fig. 2). At $T/t = 0.005$ the antiferromagnetic (AFM) order is progressively reduced increasing V/t as shown in

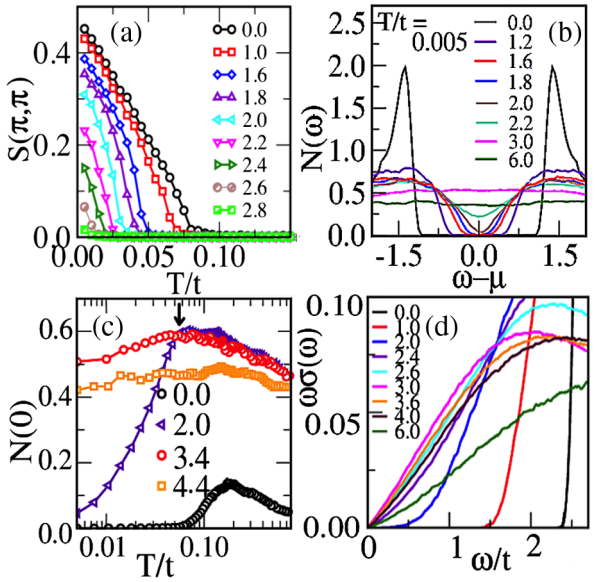

FIG. 2. Examples of MFMC data at $U/t = 4$ used to construct the phase diagram of Fig. 1. (a) Static magnetic structure factor at $q = (\pi, \pi)$. Values of V/t are in the column. (b) Low-T DOS $N(\omega)$ at various disorder strengths. (c) DOS $\omega = 0$ weight at the four V/t's indicated versus T/t. The arrow indicates the maximum of $N(0)$ for $V/t = 3.4$. (d) ω times the optical conductivity $\sigma(\omega)$, at $T/t = 0.005$, for the several V/t's indicated.

Fig. 2(a), and for $V \geq 2.6t$ the signal becomes negligible. At $V = 0$, the magnetic order starts at $T/t = 0.10$ upon cooling but the system remains insulating above this temperature, as expected, and a paramagnetic insulator (PMI) is deduced based on the optical conductivity behavior discussed below. Increasing V/t, T_N initially slightly increases and then reduces with increasing disorder [53]. The metal insulator boundary decreases roughly linearly with V/t, collapsing to zero at $V/t = 2.6$. Figure 2(b) shows the low-T DOS $N(\omega)$ for various disorder strengths. We find that the clean-limit Mott gap evolves into a pseudogap gap at $V/t \sim 2$. This pseudogap persists up to $V/t = 2.8$ and flattens out for larger V/t, with the weight around $\omega = 0$ decreasing gradually with disorder as the DOS spreads over a larger energy range due to increasing scattering. Thus, the AFM insulator (AFI), paramagnetic metal (PMM), and correlated Anderson insulator (CAI) phases in Fig. 1 are gapless.

Figure 2(d) shows $\omega\sigma(\omega)$ at $T = 0$ for different disorder values covering the Mott Insulator, the strange metal, and the large disorder (CAI) phases. For $V/t \leq 2.0$, $\sigma(\omega)$ is clearly gapped. In the narrow range $2.0 < V/t < 2.6$, $\omega\sigma(\omega)$ tends to zero as $\omega \to 0$ in a nonlinear manner. For $2.6 \leq V/t \leq 3.8$, $\omega\sigma(\omega) \to 0$ linearly; i.e., $\sigma(\omega)$ is constant at small ω indicating a metal. For the CAI, variable range hopping is expected to provide a $\omega^3 \ln^3(I/\omega)$ behavior [20], where I is a typical energy scale depending on the localization length. Figure 3 in Sec. II of the Supplemental Material that discusses our optical conductivity results [54]

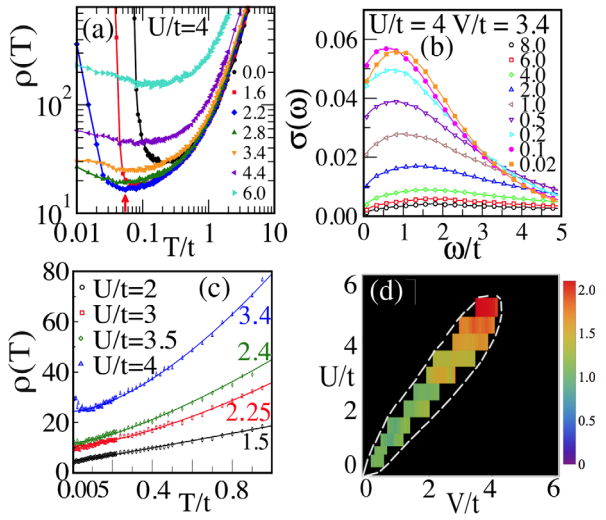

FIG. 3. (a) ρ ($\pi e^2/\hbar a_0$ units) versus T/t at $U/t = 4$ and the various V/t's in the column (a_0 is the lattice spacing, set to 1). The red arrow at the bottom shows $\rho_{\min}$ for $V/t = 3.4$. (b) Optical conductivity at $U/t = 4$ and $V/t = 3.4$ displaying non-Drude behavior, at the T/t's in the column. (c) $\rho(T)$ at special values of U/t and V/t such that the state is metallic almost in all the T/t range shown. Solid lines are fits to $\rho(0) + AT^{\alpha}$. For $U/t = 2$, 3, 3.5, and 4.0, and the V/t values indicated (color, right), α is 1.02, 1.35, 1.39, and 1.68, respectively. (d) The metallic window in the U-V plane at low temperature $T/t = 0.005$ is shown by the colored region (the dashed line just guides the eye). The black region denotes insulator. The color of the metallic region depicts the value of α arising from the T^{α} scaling of $\rho(T)$.

shows that the same behavior holds across the finite T insulator to metal transitions as well. This numerical criterion, certain subtleties, and consistency with the inverse participation ratio (IPR) are also discussed in Sec. II of the Supplemental Material [54]. We have used this criterion to determine all metal insulator boundaries in Fig. 1. Our $T = 0$ phase boundaries are in excellent agreement with earlier literature [31,57] and our metal and insulating phases both at zero and finite temperatures are robust against finite size scaling (Supplemental Material, Fig. 4 [54]). We now shift the focus to our main contributions at finite T.

Non-Fermi liquid metal.—The resistivity extracted from $1/\sigma(\omega)$ at small ω (see Supplemental Material [54]) is in Fig. 3(a) for $U/t = 4$. There are several important features. (i) $d\rho/dT$ becomes positive at large T for all values of V/t. (ii) For the PMI regime at $V/t = 0$ and 1.6, $d\rho/dT$ becomes negative with eventual divergence at the critical AFM temperature. Further, based on the optical conductivity behavior (Supplemental Material, Sec. II [54]) and finite DOS weight at the Fermi energy [$N(0)$] beyond $T/t = 0.08$ for $V = 0$ in Fig. 2(c), the PMI is a gapless insulator. For the metallic ($V/t = 2.8$ and 3.4) and the CAI ($V/t = 4.4$ and 6.6) phases, $\rho(T)$ saturates at the lowest T's investigated [58]. (iii) There are resistivity minima at finite T that coincide with the corresponding location of the peaks in $N(0)$ in Fig. 2(c) at, e.g., $V/t = 3.4$. The NFL nature of the disorder-induced metallic state can be inferred from Fig. 3(b), which shows that $\sigma(\omega)$ has a non-Drude form with a peak at a finite frequency. This peak is further pushed to higher frequency with increasing T, except at very low T when the peak converges to $\omega/t \sim 1$.

Both $\rho(T)$ here and the specific heat C_v in Fig. 5 of the Supplemental Material [54] show low T deviations from FL behavior consistent with the literature on disorder induced NFLs [18], justifying our "NFL metal" nomenclature.

Consider now the ρ versus T behavior for the NFL state. In the metallic regime ($V/t = 3.4$), the resistivity minimum occurs at $T/t \sim 0.1$. From Fig. 2(c) at $V/t = 3.4$, the location of $\rho_{\min}$ coincides with the peak in $N(0)$ at $T/t \sim 0.055$. This nonmonotonic dependence of $N(0)$ on T agrees with determinantal quantum Monte-Carlo (DQMC) studies of the Hubbard model [59] for $V = 0$.

The initial increase of $N(0)$ is due to thermally induced fluctuations that enhance the DOS weight at $\omega = 0$. At high T, the scattering of fermions from the AFs suppress $N(0)$, and this nonmonotonicity is reflected in the metallic-like thermal behavior of $\rho(T)$. In summary, at low T the initial increase of the DOS at the Fermi level forces $d\rho/dT$ to be negative, while at high T this DOS is suppressed again because of the localized spins and $d\rho/dT$ changes sign.

Scaling of resistivity.—In Fig. 3(c) we show $\rho(T)$ for combinations of U/t and V/t where the system is a metal over a wide temperature range. The full map of the low temperature metallic region in the U/t-V/t plane is in Fig. 3(d). The resistivity data are fitted to $\rho(0) + AT^{\alpha}$ for each case to extract α [60]. For small or intermediate values of $(U/t, V/t)$ (open circles), $\rho(T)$ grows linearly with T in the range analyzed. For larger U/t (and corresponding V/t) α increases from ~1.0 to 1.7 for $U/t = 2, V/t = 3.4$. As shown in Fig. 3(d), the metallic window at $T/t = 0.005$ occurs roughly around the line $U \sim 1.25V$ [61]. The dashed line guides the eye and it envelops the metallic region. The metallic-regime color scale indicates the value of α in the temperature fit of $\rho(T)$. For up to $U/t = 2.5$, $\alpha \sim 1$, growing slowly with U/t (the smallest values checked are $U/t = 0.5, V/t = 0.5$). For larger $U/t, V/t > 2.5$, α grows reaching a maximum value close to 2 for $U/t = 5$ [62]. This $\alpha \sim 2$ does not imply a FL but we believe it is just one of the possible transport exponents that occurs in our system in its slow evolution. For even larger U/t, within our precision the metallic region closes. Finally, old DQMC calculations [29] show hints of such scaling, exhibiting the robustness of our results in the presence of quantum fluctuations.

Discussion.—To better understand the combined effect of disorder and interaction in the metallic phase, in Fig. 4(a) we show the variance of the local density $\{n_i\}$, defined as $\delta n(U, V, T) = \langle \sqrt{\langle n \rangle^2 - \langle n^2 \rangle} \rangle$. The outer angular brackets imply averaging over MC samples at fixed T, while the inner ones are the quantum average within a single MC

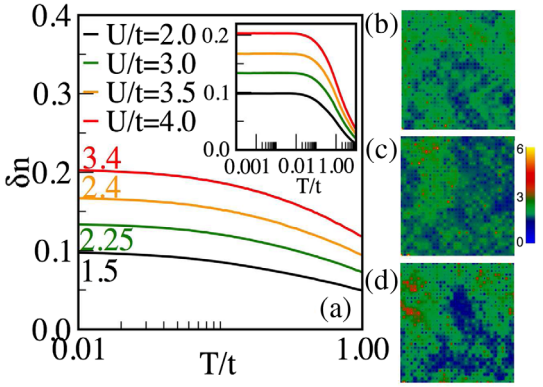

FIG. 4. Fluctuations in the charge density versus T at various U/t's and V/t's (color), in the metallic regime. The inset contains the same data up to $T/t=10$. Panels (b),(c), and (d) show real-space maps of $|\psi(r)|^2$ at the Fermi energy using 32^2 systems at $T/t = 0.2$ and coupling strengths $(U, V) = (2.0t, 1.5t), (3.0t, 2.25t)$, and $(4.0t, 3.4t)$, respectively. The color scale indicates the range of values for $|\psi(r)|^2$ in 10^{-3} units. The data in panels (a) to (d) are averaged over ten MC samples for a fixed disorder realization.

sample. There are two sources of disorder that control the variance of $\delta n(U, V, T)$. First is the static disorder (V) with variance δV and the second are the AFs. These AFs directly couple to the fermions and indirectly to the disorder through the local fermion occupations (Supplemental Material, Sec. I [39]). Then, the AFs also provide an inhomogeneous background that at low temperatures follows the presence of intrinsic static disorder. But at temperatures where $k_B T \geq \delta V$, the intrinsic disorder (V) is unimportant and the AF configurations become homogeneous in average. Thus, $\delta n(U, V, T)$ remains nonzero at low T while it tends to zero at large T, on MC sample averaging. This behavior is observed in the inset of Fig. 4(a). In the main panel we show the same data between $T/t = 0.01$ and 1. We find a systematic increase in $\delta n(U, V, T)$ with increasing U/t and V/t. This variance manifests as real-space charge clusters as shown in Figs. 4(b) to 4(d), which contain maps of $|\psi(r)|^2$ at fixed T, MC sample averaged, for states at the Fermi energy. With increasing U/t and V/t, the charge clustering and the charge fluctuation magnitude increase systematically following the increase in $\delta n(U, V, T)$. This provides a controlled enhancement in a spatially inhomogeneous background from which the fermions scatter [63].

It is known that fermions coupled to classical variables such as disorder [66], adiabatic phonons [67], etc., can exhibit charge clustering, metallic glasses, and NFL behavior. Moreover, disorder-induced rare fluctuations (of charge or spin) similar to the results in Figs. 4(b) to 4(d) are known to stabilize electronic Griffith's phases and NFL behavior [68,69] with tunable critical exponents [70].

In our case, not only the quenched disorder but also the AF fluctuations play the role of the classical scatterer that give rise to NFL scaling. Such charge clusters and NFL behavior have been experimentally observed in the 2DEG near a $T = 0$ quantum critical point [12–14]. Here, within the MFMC technique, we have found such a "charge cluster metal" in the half-filled Anderson-Hubbard model and also observed that the deviation from FL theory can be tuned. This tunability allows us to show that, in a single model Hamiltonian, the resistivity scaling with T can vary between linear to near quadratic, features observed in real NFLs like cuprates and heavy fermions. Our results thus represent progress towards identifying a single model system with NFL behavior transcending many material families.

A. M. acknowledges useful discussions with P. Majumdar, P. Chakraborty, and H. R. Krishnamurthy. N. D. P. and N. K. were supported by the National Science Foundation, under Grant No. DMR-1404375. E. D. and A. M. were supported by the U.S. Department of Energy, Office of Basic Energy Sciences, Materials Sciences and Engineering Division.

[1] P. Gegenwart, C. Langhammer, C. Geibel, R. Helfrich, M. Lang, G. Sparn, F. Steglich, R. Horn, L. Donnevert, A. Link, and W. Assmus, Phys. Rev. Lett. **81**, 1501 (1998).
[2] O. Trovarelli, C. Geibel, S. Mederle, C. Langhammer, F. M. Grosche, P. Gegenwart, M. Lang, G. Sparn, and F. Steglich, Phys. Rev. Lett. **85**, 626 (2000).
[3] S. R. Julian, C. Pfleiderer, F. M. Grosche, N. D. Mathur, G. J. McMullan, A. J. Diver, I. R. Walker, and G. G. Lonzarich, J. Phys. Condens. Matter **8**, 9675 (1996).
[4] P. Coleman, C. Pepin, Q. Si, and R. Ramazashvili, J. Phys. Condens. Matter **13**, R723 (2001).
[5] R. Jaramillo, S. D. Ha, D. M. Silevitch, and S. Ramanathan, Nat. Phys. **10**, 304 (2014).
[6] E. Lahoud, O. N. Meetei, K. B. Chaska, A. Kanigel, and N. Trivedi, Phys. Rev. Lett. **112**, 206402 (2014).
[7] A. Damascelli, Z. Hussain, and Z.-X. Shen, Rev. Mod. Phys. **75**, 473 (2003).
[8] N. E. Hussey, M. Abdel-Jawad, A. Carrington, A. P. Mackenzie, and L. Balicas, Nature (London) **425**, 814 (2003).
[9] B. Keimer, S. A. Kivelson, M. R. Norman, S. Uchida, and J. Zaanen, Nature (London) **518**, 179 (2015).
[10] P. Anderson, Nat. Phys. **2**, 626 (2006).
[11] P. A. Casey and P. W. Anderson, Phys. Rev. Lett. **106**, 097002 (2011).
[12] S. Bogdanovich and D. Popović, Phys. Rev. Lett. **88**, 236401 (2002).
[13] J. Jaroszyński, D. Popović, and T. M. Klapwijk, Phys. Rev. Lett. **89**, 276401 (2002).
[14] S. V. Kravchenko and M. P. Sarachik, Rep. Prog. Phys. **67**, 1 (2004).
[15] L. Arrachea, D. Dalidovich, V. Dobrosavljević, and M. J. Rozenberg, Phys. Rev. B **69**, 064419 (2004).
[16] D. Dalidovich and V. Dobrosavljević, Phys. Rev. B **66**, 081107 (2002).
[17] S. Sachdev and N. Read, J. Phys. Condens. Matter **8**, 9723 (1996).

[18] E. Miranda and V. Dobrosavljević, Rep. Prog. Phys. **68**, 2337 (2005).

[19] X. Deng, J. Mravlje, R. Žitko, M. Ferrero, G. Kotliar, and A. Georges, Phys. Rev. Lett. **110**, 086401 (2013).

[20] Y. Imry, *Introduction to Mesoscopic Physics* (Oxford University Press on Demand, New York, 2002).

[21] *Conductor Insulator Quantum Phase Transitions*, edited by V. Dobrosavljević, N. Trivedi, and J. M. Valles Jr. (Oxford University Press, New York, 2012).

[22] Y. Song, R. Wortis, and W. A. Atkinson, Phys. Rev. B **77**, 054202 (2008).

[23] D. Semmler, K. Byczuk, and W. Hofstetter, Phys. Rev. B **81**, 115111 (2010).

[24] D. Tanasković, V. Dobrosavljević, E. Abrahams, and G. Kotliar, Phys. Rev. Lett. **91**, 066603 (2003).

[25] M. C. O. Aguiar, V. Dobrosavljević, E. Abrahams, and G. Kotliar, Physica (Amsterdam) **403B**, 1417 (2008).

[26] K. Byczuk, W. Hofstetter, and D. Vollhardt, Phys. Rev. Lett. **102**, 146403 (2009).

[27] Y. Otsuka and Y. Hatsugai, J. Phys. Condens. Matter **12**, 9317 (2000).

[28] B. Srinivasan, G. Benenti, and D. L. Shepelyansky, Phys. Rev. B **67**, 205112 (2003).

[29] P. B. Chakraborty, P. J. H. Denteneer, and R. T. Scalettar, Phys. Rev. B **75**, 125117 (2007).

[30] R. Kotlyar and S. Das Sarma, Phys. Rev. Lett. **86**, 2388 (2001).

[31] D. Heidarian and N. Trivedi, Phys. Rev. Lett. **93**, 126401 (2004).

[32] H. Braganca, M. C. O. Aguiar, J. Vučičević, D. Tanasković, and V. Dobrosavljević, Phys. Rev. B **92**, 125143 (2015).

[33] C. E. Ekuma, S.-X. Yang, H. Terletska, K.-M. Tam, N. S. Vidhyadhiraja, J. Moreno, and M. Jarrell, Phys. Rev. B **92**, 201114 (2015).

[34] S. V. Kravchenko, W. E. Mason, G. E. Bowker, J. E. Furneaux, V. M. Pudalov, and M. D'Iorio, Phys. Rev. B **51**, 7038 (1995).

[35] D. D. Sarma, A. Chainani, S. R. Krishnakumar, E. Vescovo, C. Carbone, W. Eberhardt, O. Rader, C, Jung, C. Hellwig, W. Gudat, H, Srikanth, and A. K. Raychaudhuri, Phys. Rev. Lett. **80**, 4004 (1998).

[36] S. Nakatsuji, V. Dobrosavljević, D. Tanasković, M. Minakata, H. Fukazawa, and Y. Maeno, Phys. Rev. Lett. **93**, 146401 (2004).

[37] L. Sanchez-Palencia and M. Lewenstein, Nat. Phys. **6**, 87 (2010).

[38] While our many-body techniques capture order-parameter fluctuations, they do not include spin-flip processes characteristics of Kondo screening effects of local moments see, e.g., E. Miranda, V. Dobrosavljevic, and G. Kotliar, Phys. Rev. Lett. **78**, 290 (1997); S. Sen, H. Terletska, J. Moreno, N. S. Vidhyadhiraja, and M. Jarrell, Phys. Rev. B **94**, 235104 (2016). Thus, our effort is complementary to other previous calculations.

[39] See Supplementa1 Material, Sec. I, at http://link.aps.org/supplemental/10.1103/PhysRevLett.119.086601 for a discussion of our method [40], its numerical implementation and parallelization [41,42], its applications to various many body problems [43–49], and comparisons with determinantal quantum Monte Carlo results [50,51].

[40] A. Mukherjee, N. D. Patel, S. Dong, S. Johnston, A. Moreo, and E. Dagotto, Phys. Rev. B **90**, 205133 (2014).

[41] S. Kumar and P. Majumdar, Eur. Phys. J. B **50**, 571 (2006).

[42] A. Mukherjee, N. D. Patel, C. Bishop, and E. Dagotto, Phys. Rev. E **91**, 063303 (2015).

[43] R. Tiwari and P. Majumdar, Europhys. Lett. **108**, 27007 (2014).

[44] N. Swain, R. Tiwari, and P. Majumdar, Phys. Rev. B **94**, 155119 (2016).

[45] M. Karmakar and P. Majumdar, Phys. Rev. A **93**, 053609 (2016).

[46] S. Tarat and P. Majumdar, Eur. Phys. J. B **88**, 68 (2015).

[47] M. Karmakar and P. Majumdar, Eur. Phys. J. D **70**, 220 (2016).

[48] A. Mukherjee, N. D. Patel, A. Moreo, and E. Dagotto, Phys. Rev. B **93**, 085144 (2016).

[49] N. Swain and P. Majumdar, arXiv:1610.00695.

[50] R. Staudt, M. Dzierzawa, and A. Muramatsu, Eur. Phys. J. B **17**, 411 (2000).

[51] T. Paiva, R. T. Scalettar, C. Huscroft, and A. K. McMahan, Phys. Rev. B **63**, 125116 (2001).

[52] Our 2D magnetic T_N correspond to correlation length $\xi(T_N) \approx (L)$ (the system size). There is no T_N in 2D with an $O(3)$ auxiliary field in $L \to \infty$.

[53] The slight upturn in T_N at small V/t is compatible with the discussion in M. Ulmke, V. Janis, and D. Vollhardt, Phys. Rev. B **51**, 10411 (1995).

[54] See Supplemental Material, Sec. II, at http://link.aps.org/supplemental/10.1103/PhysRevLett.119.086601, which also includes details of our optical conductivity calculations based on the Kubo-Greenwood formalism [55] and its previous benchmarks [56].

[55] G. D. Mahan, *Quantum Many Particle Physics* (Plenum Press, New York, 1990).

[56] S. Kumar and P. Majumdar, Eur. Phys. J. B **46**, 237 (2005).

[57] D. Heidarian, Ph.D. thesis, School of Natural Sciences Tata Institute of Fundamental Research Mumbai, 2006.

[58] Since our calculation is on a finite system and the lowest temperature accessed is $T = 0.005t$, the expected divergence in $\rho(T)$ as $T \to 0$ for the CAI is not captured. Thus, the optical conductivity data are the best indicator of metal versus insulator.

[59] T. Paiva, Y. L. Loh, M. Randeria, R. T. Scalettar, and N. Trivedi, Phys. Rev. Lett. **107**, 086401 (2011).

[60] There is a also a variation in α with V for a fixed U; details will be reported elsewhere as this is not the central issue being addressed here.

[61] In the absence of quantum ($t=0$) and thermal ($T=0$) fluctuations, the line $U=V$ is special, separating a phase with all sites singly occupied from another phase with a mixture of occupancies. This is why our metallic phase is close to $U = V$.

[62] A resistivity minimum occurs for all the cases but is pushed to lower temperatures for smaller U, so the fitting is done in the regime where $d\rho/dT > 0$ going up to $T/t = 1$.

[63] Extensions of the present work may include other forms of disorder (hoppings, etc.) as explored in the literature [64,65].

[64] P. J. H. Denteneer, R. T. Scalettar, and N. Trivedi, Phys. Rev. Lett. **87**, 146401 (2001).

[65] P. J. H. Denteneer and R. T. Scalettar, Phys. Rev. Lett. **90**, 246401 (2003).
[66] S. Kumar and P. Majumdar, Phys. Rev. Lett. **94**, 136601 (2005).
[67] S. Blawid, A. Deppeler, and A. J. Millis, Phys. Rev. B **67**, 165105 (2003).
[68] E. C. Andrade, E. Miranda, and V. Dobrosavljević, Phys. Rev. Lett. **102**, 206403 (2009).
[69] M. Milovanović, S. Sachdev, and R. N. Bhatt, Phys. Rev. Lett. **63**, 82 (1989).
[70] E. Miranda and V. Dobrosavljević, Phys. Rev. Lett. **86**, 264 (2001).